A new adjustable localization operator method to compute local stresses and strains at notched bodies under multiaxial cyclic loading

Ewann Gautier, Bruno Levieil, Sylvain Calloch, Cédric Doudard

A New Adjustable Localization Operator Method to Compute Local Stresses and Strains at Notched Bodies under Multiaxial Cyclic Loading

Ewann Gautier[a,*], Bruno Levieil[a], Sylvain Calloch[a], Cédric Doudard[a]

[a] *2 rue François Verny, ENSTA Bretagne, UMR CNRS 6027, IRDL, F-29200 Brest, France*

Abstract

Simplified methods for elastoplastic calculations offer a cost-effective and time-saving solution to determine the mechanical state at the notch tip of a structure. Recently, a method using an Adjustable Localization Operator (ALO) has been developed, drawing inspiration from Eshelby's inclusion problem. This method has demonstrated its efficiency in addressing various engineering challenges owing to its robustness and inherent ability to handle multiaxial conditions. This paper aims to propose an alternative non-linear formulation of the ALO method to improve the accuracy of mechanical state predictions. To achieve this goal, Buczynski-Glinka's heuristic, which provides a non-linear plasticity correction, is expressed within the framework of the ALO method to highlight the ingredients required for a non-linear plastic correction. Subsequently, the parameters of the ALO method are adjusted based on these findings. To validate the approach, two cases are studied: a notched structure under plain strain conditions, and a more complex saddle notched structure subjected to local multiaxial proportional loadings. In both cases, the non-linear ALO method has shown a greater capability to reproduce the finite element reference results compared to the linear version of the method or to energetic methods.

Keywords: Nonlinear plastic correction, Energetic methods, Cyclic plasticity, Confined plasticity, Neuber's rule

Nomenclature

$\underline{\underline{\sigma}}$	Stress tensor for an elasto-plastic behavior	$\underline{\underline{\varepsilon}}$	Strain tensor for an elasto-plastic behavior
$\underline{\underline{\varepsilon}}^e$	Elastic strain tensor for elasto-plastic behavior	$\underline{\underline{\varepsilon}}^p$	Plastic strain tensor for elasto-plastic behavior
$\underline{\underline{\Sigma}}$	Stress tensor for an elastic behavior	$\underline{\underline{\mathbb{E}}}$	Strain tensor for an elastic behavior

*Corresponding author
Email address: ewann.gautier@ensta-bretagne.org (Ewann Gautier)

$\underline{\underline{S}}$	Deviatoric stress tensor for an elastic behavior	$\underline{\underline{E}}$	Deviatoric strain tensor for an elastic behavior
$d\lambda$	Plastic multiplier	$E_{N_{ij}}$	Neuber's energy
$\underline{\underline{s}}$	Deviatoric stress tensor for an elasto-plastic behavior	$\underline{\underline{e}}$	Deviatoric strain tensor for an elasto-plastic behavior
$\underline{\underline{\underline{\underline{J}}}}$	Deviatoric projector	Δ	Difference with a memory point
E	Young modulus	ν	Poisson's ratio
μ	Shear modulus	$\underline{\underline{I}}$	Identity matrix
$\underline{\underline{\underline{\underline{L}}}}^{ALO}$	Adjustable Localization Operator	β	Eshelby's parameter
z_{ij}	Parameters of the adjustable localization operator	δ_{ij}	Kronecker symbol
$\underline{\underline{\underline{\underline{L}}}}^{BG}$	Buczynski-Glinka operator	$\underline{\underline{F}}^{BG}$	Buczynski-Glinka tensor
$\underline{\underline{\underline{\underline{L}}}}^{BG}_{mod}$	Modified Buczynski-Glinka operator	σ^{VM}	von Mises equivalent stress
$\underline{\underline{X}}_i$	i-th kinematic hardening	C_i	Parameter for i-th kinematic hardening
J_2	Second invariant of the deviatoric stress tensor	γ_i	Parameter for i-th kinematic hardening
f	Yield surface	σ_y	Yield stress

1. Introduction

During service life, industrial parts experience cyclic loads that can lead to fatigue failure. The presence of concentrated stress areas exacerbates this phenomenon, contributing to the development of limited scale yielding or confined plasticity. Such cyclic plastic behavior in these specific areas can cause premature failure, in the Low-Cycle Fatigue domain. Consequently, accurately knowing the stress state is crucial for determining the appropriate structural dimensions and estimating the lifespan of these structures.

Although finite element analysis (FEA) is suitable for performing elastic calculations on structures, it may not be the optimal approach for studying confined plasticity. This is mainly due to the considerable computational cost associated with simulating each cycle by considering the elastoplastic behavior at critical locations in the structure. Additionally, a significant number of cycles needs to be simulated to achieve a stabilized behavior, further adding to the computational cost. Consequently, several alternative methods have been proposed to estimate the stress state [1–22] for various application [23–30].

Among the various methods proposed, two distinct approaches that specifically focus on the stress and strain state at critical points have gained particular interest: energetic methods [1, 4] and more recently, methods based on an adjustable localization operator (ALO) [31–33]. Figure 1 illustrates these two types of methods. By using elastic calculations, these methods allow for the

implementation of plastic corrections to determine the elastoplastic behavior at critical points of structural parts.

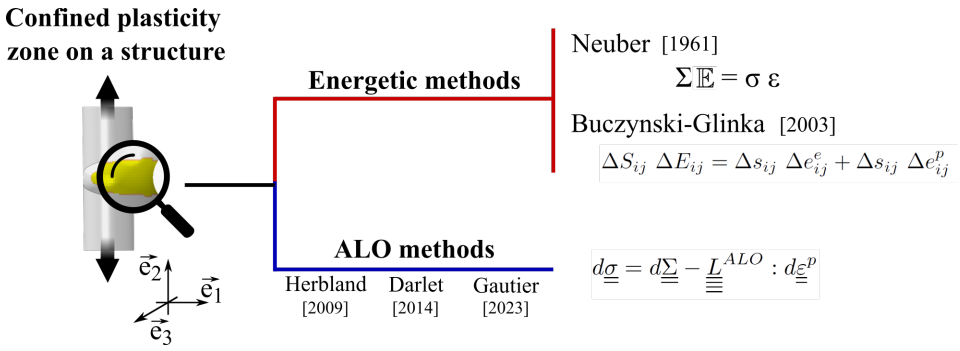

Figure 1: Diagram of energetic méthods and ALO methods with $\underline{\underline{\Sigma}}$ and $\underline{\underline{\mathbb{E}}}$ the stress and strain tensor for an elastic simulation, $\underline{\underline{\sigma}}$ and $\underline{\underline{\varepsilon}}$ the stress and strain tensor for an elastoplastic simulation, $\underline{\underline{\underline{\underline{L}}}}^{ALO}$ the adjustable localization operator, and $\underline{\underline{S}}$, $\underline{\underline{E}}$, $\underline{\underline{s}}$ and $\underline{\underline{e}}$ the deviatoric parts of the previous tensors.

In 1961, Neuber [1] established that the energy density remains independent of plastic flow, making it equivalent for both elastic and elastoplastic behavior. This rule was initially demonstrated in the case of shear force applied to a prism. However, Neuber's rule is limited to uniaxial loading conditions and cannot be directly extended to cases involving multiaxial loading. For instance, when considering an axisymmetric notched specimen, a total of nine variables are required to describe the material state in the principal stress and strain space at the critical point on its surface. These variables are listed in table 1.

Table 1: Variables of the confined plasticity problem

Definition of variables	
Stress tensor variables	$\sigma_{11},\ \sigma_{22},\ \sigma_{33}$
Strain tensor variables	$\varepsilon_{11},\ \varepsilon_{22},\ \varepsilon_{33}$
Plastic strain tensor variables	$\varepsilon^p_{11},\ \varepsilon^p_{22},\ \varepsilon^p_{33}$

Therefore, solving this multiaxial problem requires nine equations. However, only seven equations are commonly available (table 2) and even with Neuber's rule providing an additional equation, one equation is still missing. Consequently, several studies have proposed different heuristics to extend the application of Neuber's rule to a more general case, specifically for multiaxial stress states [34–39]. Amongst these proposals, Buczynski-Glinka [38] introduced an original heuristic that applies Neuber's concept to each component of the stress and strain tensors using their deviators. This solution provides a specific multiaxial formalism for Neuber's rule.

Table 2: Equations available with Neuber's methods for confined plasticity problem

Name	Number of equations	Equations
Hooke's law	3	$\underline{\underline{\sigma}} = \underline{\underline{\underline{\underline{C}}}} : (\underline{\underline{\varepsilon}} - \underline{\underline{\varepsilon}}^p)$
Plastic flow	3	$\dot{\underline{\underline{\varepsilon}}}^p = f(\underline{\underline{\sigma}}, \underline{\underline{\varepsilon}}^p, \dot{\underline{\underline{\sigma}}})$
Boundary condition (with $\vec{e_1}$ being the normal)	1	$\sigma_{11} = 0$

More recently, a method based on an adjustable localization operator has been developed, assuming that under the limited scale yielding assumption, the confined plasticity zone behaves as an elastoplastic inclusion in an elastic matrix. Different strategies for identifying the operator have been detailed in the literature [31–33]. The formalism of the adjustable localization operator is based on the Eshelby tensor, a fourth-order tensor. By drawing an analogy with the Kröner-Eshelby inclusion problem [40, 41] and with some simplifications and assumptions (detailed later in the paper), there is only five parameters left to be determined [33, 42].

Several studies have highlighted the effectiveness of these methods in determining the stress state at critical points. These studies have been conducted on welded joints [43], notched structures under different load ratios [44], various residual stress states [45], and for multiaxial and non-proportional loadings [33]. The method has also been extended to materials with anisotropic yield surfaces [46]. Fatigue lives, as well as predicted stress and strain stabilized states, have been determined and compared with experimental data and finite element predictions, validating their reliability and accuracy.

This method is inherently multiaxial, and its formalism enables efficient numerical integration. Furthermore, this method can be effectively combined with Darlet's multiaxial heuristic [32, 42], as demonstrated in previous studies [33, 42], which is essential for the evolution of the stress ratio. However, it is important to acknowledge a limitation of this method, which lies in its linear plastic correction, as illustrated in figure 2. The figure showcases the difference between the von Mises equivalent stress obtained from elastic simulation and elastoplastic simulation for a 2D notched specimen under plane stress conditions. Although the adjustable localization operator method provides accurate predictions [33], the plastic correction exhibits a linear evolution, contrasting with the non-linear behavior observed for finite element analysis and Neuber's rule.

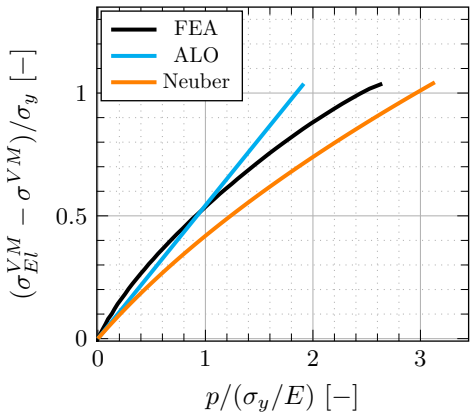

Figure 2: Evolution of the difference between the von Mises equivalent stress from the elastic simulation and the elastoplastic simulation

The objective of this study is to justify a new structure of the adjustable localization operator by engaging in a dialogue with an energetic method. This connection aims to showcase the feasibility of introducing a novel operator that can provide a non-linear plastic correction, thereby reducing the error when compared to finite element analysis.

The paper is divided into four sections. The first section describes the Buczynski-Glinka heuristic and highlights its differences from Neuber's rule. In the second section, the parameters of the adjustable localization operator are determined rewriting the Buczynski-Glinka energetic approach in a similar form. The third section introduces an original adjustable localization operator which possesses parameters that are not constants. This achievement is made possible by leveraging the insights provided by the Buczynski-Glinka approach and incorporating Darlet's multiaxial heuristic. Finally, this non-linear plastic correction is tested under local proportional multiaxial loadings. The performance of the method is evaluated by comparing its results with those obtained from finite element solutions.

2. Energetic methods for local elasto-plastic predictions

2.1. Neuber's rule and its evolution

As stated in the introduction, nine equations are necessary to determine the three elasto-plastic tensorial variables in the principal basis (total strain, plastic strain and stress). Classic formulations provide seven equations sum up in table 2. Neuber's rule provides an additional equation.

To generalize Neuber's rule to various configurations, several propositions have been made in the literature [34–39]. For example, using the second invariant of stress and strain in the deviatoric space J_2

$$E_N = J_2(\underline{\underline{\mathbb{E}}})\ J_2(\underline{\underline{\Sigma}}) = J_2(\underline{\sigma})\ J_2(\underline{\varepsilon})\ , \tag{1}$$

where $\underline{\underline{\mathbb{E}}}$ and $\underline{\underline{\Sigma}}$ are the variables associated respectively to the strain and stress tensors of an elastic behavior, and where $\underline{\varepsilon}$ and $\underline{\sigma}$ are those assuming an elasto-plastic behavior [1]. The expression of

the second invariant of stress in the deviatoric space is given by

$$J_2(\underline{\underline{\Sigma}}) = \sqrt{\frac{3}{2}\,\underline{\underline{S}} : \underline{\underline{S}}}\,, \tag{2}$$

with $\underline{\underline{S}}$ the deviatoric stress tensor. The total strain $\underline{\underline{\varepsilon}}$ is the sum of the elastic and plastic strains and is written

$$\underline{\underline{\varepsilon}} = \underline{\underline{\varepsilon}}^e + \underline{\underline{\varepsilon}}^p\ . \tag{3}$$

It should be noted that, in this paper, the plastic flow is obtained by using the normality rule

$$d\underline{\underline{\varepsilon}}^p = d\lambda \frac{\partial f}{\partial \underline{\underline{\sigma}}}\ , \tag{4}$$

with $d\lambda$ the plastic multiplier and f the yield surface. Using the modified Voigt notation, the stress and strain tensors are written in all this article

$$\underline{\underline{\sigma}} = \begin{bmatrix} \sigma_{11} \\ \sigma_{22} \\ \sigma_{33} \\ \sigma_{23}\sqrt{2} \\ \sigma_{13}\sqrt{2} \\ \sigma_{12}\sqrt{2} \end{bmatrix} \text{ and } \underline{\underline{\varepsilon}} = \begin{bmatrix} \varepsilon_{11} \\ \varepsilon_{22} \\ \varepsilon_{33} \\ \varepsilon_{23}\sqrt{2} \\ \varepsilon_{13}\sqrt{2} \\ \varepsilon_{12}\sqrt{2} \end{bmatrix}\ . \tag{5}$$

However, the equation Eq. 2 is not sufficient to solve the problem completely. As previously mentioned, in the case of a multiaxial problem solved in the stress principal basis, a ninth equation is needed. To provide the ninth equation, several propositions have been formulated [34–37, 39].

2.2. Buczynski-Glinka's heuristic

Buczynski-Glinka's proposal [38] is completely different, since it involves writing Neuber's rule component by component, using the deviatoric strain and stress tensors. Einstein's convention **is not used**. The equation proposed by Buczynski-Glinka is

$$\forall (i,j) \in [\![1,3]\!], \Delta E_{N_{ij}} = \Delta S_{ij}\ \Delta E_{ij} = \Delta s_{ij}\ \Delta e^e_{ij} + \Delta s_{ij}\ \Delta e^p_{ij} \tag{6}$$

where

$$\begin{cases} \underline{\underline{E}} = \underline{\underline{\underline{\underline{J}}}} : \underline{\underline{\mathbb{E}}} \\ \underline{\underline{S}} = \underline{\underline{\underline{\underline{J}}}} : \underline{\underline{\Sigma}} \\ \underline{\underline{e}} = \underline{\underline{\underline{\underline{J}}}} : \underline{\underline{\varepsilon}} \\ \underline{\underline{s}} = \underline{\underline{\underline{\underline{J}}}} : \underline{\underline{\sigma}} \end{cases}\ ,$$

and $\underline{\underline{\underline{\underline{J}}}}$ is the deviatoric projector. The notation Δ designates the variation of the variables with respect to a memory point, necessary when using Neuber's rule for cyclic loading. This memory point is updated when the loading direction changes, as illustrated in figure 3.

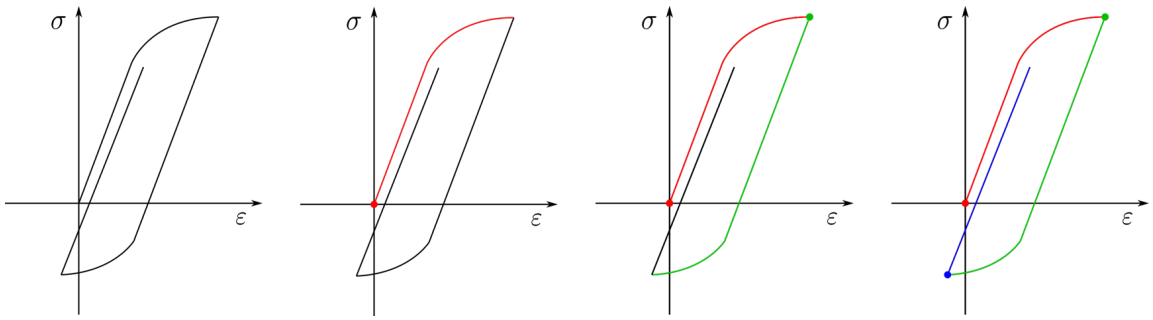

Figure 3: Definition of the memory point to apply Neuber's rule for cyclic loading

Since $\underline{\underline{\varepsilon^p}}$ is deviatoric, its deviator $\underline{\underline{e^p}}$ is directly

$$\underline{\underline{e^p}} = \underline{\underline{\varepsilon^p}} \ . \tag{7}$$

The deviatoric formulation of the elastic strain tensor $\underline{\underline{\mathbb{E}}}$ (using the elastic behavior) is obtained by writing the isotropic Hooke's law

$$\begin{aligned} \underline{\underline{\mathbb{E}}} &= \frac{1+\nu}{E}\ \underline{\underline{\Sigma}} - \frac{\nu}{E}\ Tr(\underline{\underline{\Sigma}})\ \underline{\underline{I}} \\ &= \frac{1+\nu}{E}\ (\underline{\underline{S}} + \frac{1}{3}\ Tr(\underline{\underline{\Sigma}})\ \underline{\underline{I}}) - \frac{\nu}{E}\ Tr(\underline{\underline{\Sigma}})\ \underline{\underline{I}} \\ &= \frac{1+\nu}{E}\ \underline{\underline{S}} + (\frac{1+\nu}{3E} - \frac{\nu}{E})\ Tr(\underline{\underline{\Sigma}})\ \underline{\underline{I}} \ , \end{aligned} \tag{8}$$

where the deviator of the elastic strain is

$$\underline{\underline{E}} = \frac{1+\nu}{E}\ \underline{\underline{S}} = \frac{1}{2\mu}\ \underline{\underline{S}} \ , \tag{9}$$

with μ the second Lamé coefficient (shear modulus), E the Young modulus and ν the Poisson's ratio. This also applies to the deviatoric elastic strain calculated using an elasto-plastic behavior that is written

$$\underline{\underline{e}}^e = \frac{1+\nu}{E}\ \underline{\underline{S}} = \frac{1}{2\mu}\ \underline{\underline{s}} \ , \tag{10}$$

It should be noted, however, that the proposal of this multiaxial heuristic is slightly different from Neuber's rule when applied to a case of uniaxial tension in plane stress. Considering direction 2 as the direction of loading for a tensile test, the Neuber equation is written

$$\Sigma_{22}\ \mathbb{E}_{22} = \sigma_{22}\ \varepsilon_{22} = \sigma_{22}\ (\varepsilon^e_{22} + \varepsilon^p_{22}) \ . \tag{11}$$

The Buczynski-Glinka equation is given by

$$S_{22}\ E_{22} = s_{22}\ e_{22} = s_{22}\ (e^e_{22} + \varepsilon^p_{22}) \ . \tag{12}$$

and can be rewritten in terms of stresses and strains (and not their deviatoric formulations). The Eq. 12 then becomes

$$\frac{2}{3}\Sigma_{22}\ \frac{1}{2\mu}\frac{2}{3}\Sigma_{22} = \frac{2}{3}\sigma_{22}(\frac{1}{2\mu}\frac{2}{3}\sigma_{22} + \varepsilon^p_{22}) \ , \tag{13}$$

$$\Sigma_{22}\ \frac{2}{3}\frac{1+\nu}{E}\Sigma_{22} = \sigma_{22}\left(\frac{2}{3}\frac{1+\nu}{E}\sigma_{22} + \varepsilon^p_{22}\right)\ , \tag{14}$$

$$\Sigma_{22}\ \frac{2}{3}(1+\nu)\ E_{22} = \sigma_{22}\left(\frac{2}{3}(1+\nu)\varepsilon^e_{22} + \varepsilon^p_{22}\right)\ . \tag{15}$$

The following relationship is then obtained

$$\Sigma_{22}\ E_{22} = \sigma_{22}\varepsilon^e_{22} + \sigma_{22}\varepsilon^p_{22}\frac{3}{2(1+\nu)}\ . \tag{16}$$

The proposed heuristic by Buczynski-Glinka offers an interesting approach as it enables a multiaxial formulation of Neuber's rule. However, there are slight differences between the two approaches, particularly when the Poisson's ratio (ν) is not equal to 0.5. In the Buczynski-Glinka approach, the plastic strain is multiplied by the term $\frac{3}{2(1+\nu)}$, which sets it apart from Neuber's rule.

These energetic methods are also interesting as they directly offer a non-linear correction as it allows for a better description of the mechanical state in some configurations (figure 2).

The ALO method can offer a linear or non-linear correction. So far, the non-linear correction has only been explored by Herbland [31] and Chouman [47]. However, in their proposition, the calibration of the operator requires an elasto-plastic finite element model, which is not always available. In more recent publications [33, 42], only a linear elastic finite element model is required. However, so far, only a linear correction has been explored. The objective of the rest of the paper is to rewrite Buczynksi-Glinka proposition in order to link it to the ALO method and thus to propose a non-linear version of the ALO method.

3. Dialog between Buczynski-Glinka method and ALO methods

The current section firstly introduces the ALO method before to rewrite Buczynski-Glinka method with a similar formalism. The two methods are then compared to the finite element reference results on a case study to show their performance and highlight their linear or non-linear behaviors within the specific plane depicted in figure 2.

3.1. Adjustable Localization Operator formalism

The localization equation used in this ALO method is

$$d\underline{\underline{\sigma}} = d\underline{\underline{\Sigma}} - \underline{\underline{\underline{\underline{L}}}}^{ALO} : d\underline{\underline{\varepsilon}}^p\ \ . \tag{17}$$

where $d\underline{\underline{\varepsilon}}^p_{loc}$ is the increment of local plastic strain and $\underline{\underline{\underline{\underline{L}}}}^{ALO}$ is the fourth-order operator used to apply the plastic correction. Considering the direction $\vec{1}$ as the normal to the surface, the strain and stress tensors are written

$$\underline{\underline{\sigma}} = \begin{bmatrix} 0 \\ \sigma_{22} \\ \sigma_{33} \\ \sigma_{23}\sqrt{2} \\ 0 \\ 0 \end{bmatrix} \text{ and } \underline{\underline{\varepsilon}} = \begin{bmatrix} \varepsilon_{11} \\ \varepsilon_{22} \\ \varepsilon_{33} \\ \varepsilon_{23}\sqrt{2} \\ \varepsilon_{13}\sqrt{2} \\ \varepsilon_{12}\sqrt{2} \end{bmatrix}\ . \tag{18}$$

The expression of the ALO operator is

$$\underline{\underline{\underline{\underline{L}}}}^{ALO} = \begin{pmatrix} L_{1111} & L_{1122} & L_{1133} & L_{1123} & L_{1113} & L_{1112} \\ L_{2211} & L_{2222} & L_{2233} & L_{2223} & L_{2213} & L_{2212} \\ L_{3311} & L_{3322} & L_{3333} & L_{3323} & L_{3313} & L_{3312} \\ L_{2311} & L_{2322} & L_{2333} & L_{2323} & L_{2313} & L_{2312} \\ L_{1311} & L_{1322} & L_{1333} & L_{1323} & L_{1313} & L_{1312} \\ L_{1211} & L_{1222} & L_{1233} & L_{1223} & L_{1213} & L_{1212} \end{pmatrix}_{(\vec{e_1},\vec{e_2},\vec{e_3})} . \tag{19}$$

As a confined plasticity zone is considered, the following simplifications and assumptions can be made:

- The free-edge boundary condition with the normal direction $\vec{e_1}$;
- The plastic incompressibility;
- No couplings between shear and normal stress terms.

Consequently, the fourth-order ALO operator can be rewritten as follows

$$\underline{\underline{\underline{\underline{L}}}}^{ALO} = \begin{pmatrix} 0 & 0 & 0 & 0 & 0 & 0 \\ 0 & L_{2222} & L_{2233} & 0 & 0 & 0 \\ 0 & L_{3322} & L_{3333} & 0 & 0 & 0 \\ 0 & 0 & 0 & L_{2323} & 0 & 0 \\ 0 & 0 & 0 & 0 & 0 & 0 \\ 0 & 0 & 0 & 0 & 0 & 0 \end{pmatrix}_{(\vec{e_1},\vec{e_2},\vec{e_3})} , \tag{20}$$

or

$$\underline{\underline{\underline{\underline{L}}}}^{ALO} = 2\mu(1-\beta) \begin{pmatrix} 0 & 0 & 0 & 0 & 0 & 0 \\ 0 & z_{22} & z_{23} & 0 & 0 & 0 \\ 0 & z_{32} & z_{33} & 0 & 0 & 0 \\ 0 & 0 & 0 & z_{44} & 0 & 0 \\ 0 & 0 & 0 & 0 & 0 & 0 \\ 0 & 0 & 0 & 0 & 0 & 0 \end{pmatrix}_{(\vec{e_1},\vec{e_2},\vec{e_3})} , \tag{21}$$

where β is the Eshelby's parameter, μ the shear modulus and z_{22}, z_{33}, z_{23}, z_{32} and z_{44} are five parameters to identify.

The parameters z_{ij} are the key parameters to be determined [31, 33, 42]. These parameters are dependent on the geometry, loading directions, and material properties. In the most recent version of the method [33], the shape of the confined plasticity zone is also considered to enhance the predictive capabilities. However, for the purpose of this paper, which focuses on establishing a dialogue between the ALO method and the Buczynski-Glinka heuristic, the version proposed by Darlet is more appropriate. As demonstrated in this paper, when the Buczynski-Glinka heuristic is reformulated using the same formalism as the ALO method, it is observed that z_{22} and z_{33} are equal, as in Darlet's proposition, which is not the case in the more recent version of the method.

The following two sections aim to introduce a tensorial notation of the Buczynski-Glinka heuristic, resulting in a fourth-order tensor that is similar to the ALO operator.

3.2. Expression of the components of the stress and strain tensor for Buczynski-Glinka heuristic

To implement the Buczynski-Glinka heuristic in the formalism of an adjustable localization operator as presented above, it is necessary to express each component of the stress tensor $d\underline{\underline{\sigma}}_{ij}$ in function of $d\underline{\underline{s}}_{ij}$, the component of the deviatoric stress tensor.

Differentiating the Buczynski-Glinka expression (Eq. 6) in each direction, the expressions of the elastic solution (S_{ij} and E_{ij}) and the elasto-plastic solution (s_{ij} and e_{ij}) are obtained

$$\begin{aligned} dE_{N_{ij}} &= dS_{ij}\ \Delta E_{ij} + \Delta S_{ij}\ dE_{ij} \\ &= \Delta s_{ij}\ de^e_{ij} + \Delta s_{ij}\ de^p_{ij} + ds_{ij}\ (\Delta e^e_{ij} + \Delta e^p_{ij})\ . \end{aligned} \tag{22}$$

In the elastic prediction, only $dE_{N_{ij}}$ is imposed by the loading. The yield surface, f, is then calculated. If the latter remains negative or zero, the elastic prediction is verified and the next increment is processed. Otherwise, a plastic correction is applied. The relationship between $dE_{N_{ij}}$ and the elastic solution can be summarised as

$$dE_{N_{ij}} = 2\ \frac{\Delta S_{ij}}{2\ \mu}\ dS_{ij} = \frac{\Delta S_{ij}}{\mu}\ dS_{ij}\ . \tag{23}$$

On the other hand, the relation between $dE_{N_{ij}}$ and the elasto-plastic solution is reduced to

$$\begin{aligned} dE_{N_{ij}} &= \Delta s_{ij}\ de^e_{ij} + ds_{ij}\ (\Delta e^e_{ij} + \Delta \varepsilon^p_{ij}) \\ &= (\frac{\Delta s_{ij}}{2\ \mu} + \Delta \varepsilon^p_{ij} + \frac{\Delta s_{ij}}{2\ \mu})\ ds_{ij} \\ &= (\frac{\Delta s_{ij}}{\mu} + \Delta \varepsilon^p_{ij})\ ds_{ij}\ , \end{aligned} \tag{24}$$

where de^p_{ij} is removed from the equation, as the increment is a purely elastic prediction. Using these two equations yields an expression for the incremental deviatoric stress, ds_{ij}

$$ds_{ij} = \frac{\Delta S_{ij}}{\Delta s_{ij} + \mu \Delta \varepsilon^p_{ij}}\ dS_{ij}\ . \tag{25}$$

Then, in order to obtain a formulation based only on the terms S_{ij} and ε^p_{ij}, the following relationship is obtained from Eq. 6

$$\begin{aligned} \frac{\Delta S^2_{ij}}{2\ \mu} &= \frac{\Delta s^2_{ij}}{2\ \mu} + \Delta s_{ij}\ \Delta \varepsilon^p_{ij} \\ \Delta S^2_{ij} &= \Delta s^2_{ij} + \Delta s_{ij}\ (2\ \mu \Delta \varepsilon^p_{ij}) \\ \Delta S^2_{ij} + (\mu \Delta \varepsilon^p_{ij})^2 &= (\Delta s_{ij} + \mu \Delta \varepsilon^p_{ij})^2\ . \end{aligned} \tag{26}$$

Thanks to the previous equation, equation Eq. 25 is rewritten

$$ds_{ij} = dS_{ij}\ \frac{1}{\sqrt{1 + (\frac{\mu \Delta \varepsilon^p_{ij}}{\Delta S_{ij}})^2}}\ . \tag{27}$$

The Eq. 22 can be rewritten in a general case (i.e. without removing $d\varepsilon_{ij}^p$)

$$\begin{aligned} dE_{N_{ij}} &= \Delta s_{ij}\ de_{ij}^e + \Delta s_{ij}\ d\varepsilon_{ij}^p + ds_{ij}\ \Delta e_{ij} \\ &= \frac{\Delta s_{ij}}{2\ \mu}\ ds_{ij} + \Delta s_{ij}\ d\varepsilon_{ij}^p + ds_{ij}\ \Delta e_{ij} \\ &= (\frac{\Delta s_{ij}}{2\ \mu} + \Delta e_{ij})\ ds_{ij} + \Delta s_{ij}\ d\varepsilon_{ij}^p\ . \end{aligned} \tag{28}$$

Hence the following expression for ds_{ij} as a function of $d\varepsilon_{ij}^p$

$$ds_{ij} = \frac{dE_{N_{ij}}}{\frac{\Delta s_{ij}}{2\ \mu} + \Delta e_{ij}} - \frac{\Delta s_{ij}\ d\varepsilon_{ij}^p}{\frac{\Delta s_{ij}}{2\ \mu} + \Delta e_{ij}}\ . \tag{29}$$

Subsequently, the stress increment is determined by adding the spherical part, to return to the stress-strain space. The stress increment is

$$d\sigma_{ij} = ds_{ij} + \frac{1}{3}Tr(d\underline{\underline{\sigma}})\delta_{ij}\ , \tag{30}$$

with δ_{ij} the Krönecker symbol. Writing this equation for σ_{22} and assuming that direction 1 is the normal to the surface, one can obtain

$$d\sigma_{22} = ds_{22} + \frac{1}{3}(d\sigma_{22} + d\sigma_{33})\ , \tag{31}$$

yet

$$\begin{aligned} ds_{11} &= d\sigma_{11} - \frac{1}{3}(d\sigma_{11} + d\sigma_{22} + d\sigma_{33}) \\ &= -\frac{1}{3}(d\sigma_{22} + d\sigma_{33})\ , \end{aligned} \tag{32}$$

hence

$$d\sigma_{22} = ds_{22} - ds_{11}\ . \tag{33}$$

It is thus possible to formulate this equation as

$$d\sigma_{ij} = ds_{ij} - \delta_{ij} ds_{kk}\ , \tag{34}$$

with δ_{ij} the Kronecker symbol and k the direction normal to the surface, which in this paper is the direction 1. The stress increment $d\sigma_{ij}$ is then given by

$$d\sigma_{ij} = \frac{1}{\frac{\Delta s_{ij}}{2\ \mu} + \Delta e_{ij}} dE_{N_{ij}} - \delta_{ij} \frac{1}{\frac{\Delta s_{kk}}{2\ \mu} + \Delta e_{kk}} dE_{N_{kk}} + d\sigma_{ij}\Big|_{\text{Plast Corr}} \tag{35}$$

where

$$d\sigma_{ij}\Big|_{\text{Plast Corr}} = -\frac{\Delta s_{ij}\ d\varepsilon_{ij}^p}{\frac{\Delta s_{ij}}{2\ \mu} + \Delta e_{ij}} + \delta_{ij} \frac{\Delta s_{kk}\ d\varepsilon_{kk}^p}{\frac{\Delta s_{kk}}{2\ \mu} + \Delta e_{kk}} \tag{36}$$

It is important to note that $d\sigma_{ij}$ is a function of $d\varepsilon_{ij}^p$ like the expression obtained for the ALO methods. However, $d\sigma_{ij}$ is also a function of $dE_{N_{ij}}$ and not $d\Sigma_{ij}$, unlike the ALO methods. In order to reconstruct the localization operator, it is therefore necessary to combine the terms that depend on ε_{ij}^p.

3.3. Proposition of a tensorial notation for Buczynski-Glinka heuristic

The following notation is adopted

$$Y_{ij} = \frac{\Delta s_{ij}}{\frac{\Delta s_{ij}}{2\ \mu} + \Delta e_{ij}} \tag{37}$$

to simplify the reading of the equations. Taking the equation Eq. 35, the components of the stress tensor of directions ii are written

$$\begin{aligned} d\sigma_{11} &= -\frac{\Delta s_{11}\ d\varepsilon^p_{11}}{\frac{\Delta s_{11}}{2\ \mu} + \Delta e_{11}} + \frac{dE_{N_{11}}}{\frac{\Delta s_{11}}{2\ \mu} + \Delta e_{11}} - \delta_{11}\left[-\frac{\Delta s_{11}\ d\varepsilon^p_{11}}{\frac{\Delta s_{11}}{2\ \mu} + \Delta e_{11}} + \frac{dE_{N_{11}}}{\frac{\Delta s_{11}}{2\ \mu} + \Delta e_{11}}\right] \\ &= -Y_{11} d\varepsilon^p_{11} + \frac{dE_{N_{11}}}{\frac{\Delta s_{11}}{2\ \mu} + \Delta e_{11}} - \delta_{11}\left[-Y_{11} d\varepsilon^p_{11} + \frac{dE_{N_{11}}}{\frac{\Delta s_{11}}{2\ \mu} + \Delta e_{11}}\right] \\ &= 0\ , \end{aligned} \tag{38}$$

$$\begin{aligned} d\sigma_{22} &= -\frac{\Delta s_{22}\ d\varepsilon^p_{22}}{\frac{\Delta s_{22}}{2\ \mu} + \Delta e_{22}} + \frac{dE_{N_{22}}}{\frac{\Delta s_{22}}{2\ \mu} + \Delta e_{22}} - \delta_{22}\left[-\frac{\Delta s_{11}\ d\varepsilon^p_{11}}{\frac{\Delta s_{11}}{2\ \mu} + \Delta e_{11}} + \frac{dE_{N_{11}}}{\frac{\Delta s_{11}}{2\ \mu} + \Delta e_{11}}\right] \\ &= -Y_{22}\ d\varepsilon^p_{22} + Y_{11}\ d\varepsilon^p_{11} + \frac{dE_{N_{22}}}{\frac{\Delta s_{22}}{2\ \mu} + \Delta e_{22}} - \frac{dE_{N_{11}}}{\frac{\Delta s_{11}}{2\ \mu} + \Delta e_{11}}\ , \end{aligned} \tag{39}$$

$$\begin{aligned} d\sigma_{33} &= -\frac{\Delta s_{33}\ d\varepsilon^p_{33}}{\frac{\Delta s_{33}}{2\ \mu} + \Delta e_{33}} + \frac{dE_{N_{33}}}{\frac{\Delta s_{33}}{2\ \mu} + \Delta e_{33}} - \delta_{33}\left[-\frac{\Delta s_{11}\ d\varepsilon^p_{11}}{\frac{\Delta s_{11}}{2\ \mu} + \Delta e_{11}} + \frac{dE_{N_{11}}}{\frac{\Delta s_{11}}{2\ \mu} + \Delta e_{11}}\right] \\ &= -Y_{33}\ d\varepsilon^p_{33} + Y_{11}\ d\varepsilon^p_{11} + \frac{dE_{N_{33}}}{\frac{\Delta s_{33}}{2\ \mu} + \Delta e_{33}} - \frac{dE_{N_{11}}}{\frac{\Delta s_{11}}{2\ \mu} + \Delta e_{11}}\ . \end{aligned} \tag{40}$$

For the other directions, a similar expression is obtained

$$\begin{aligned} d\sigma_{23} &= -\frac{\Delta s_{23}\ d\varepsilon^p_{23}}{\frac{\Delta s_{23}}{2\ \mu} + \Delta e_{23}} + \frac{dE_{N_{23}}}{\frac{\Delta s_{23}}{2\ \mu} + \Delta e_{23}} - 0 \\ &= -Y_{23}\ d\varepsilon^p_{23} + \frac{dE_{N_{23}}}{\frac{\Delta s_{23}}{2\ \mu} + \Delta e_{23}}\ , \end{aligned} \tag{41}$$

$$d\sigma_{13} = 0\ , \tag{42}$$

and finally

$$d\sigma_{12} = 0\ . \tag{43}$$

When the plastic correction is implemented, the variable $dE_{N_{ij}}$ is zero since it has already evolved during the elastic prediction. The relation between the stress increment and the strain increment is therefore written

$$\left.d\underline{\underline{\sigma}}\right|_{\text{Plast Corr}} = -\begin{pmatrix} 0 & 0 & 0 & 0 & 0 & 0 \\ -Y_{11} & Y_{22} & 0 & 0 & 0 & 0 \\ -Y_{11} & 0 & Y_{33} & 0 & 0 & 0 \\ 0 & 0 & 0 & Y_{23} & 0 & 0 \\ 0 & 0 & 0 & 0 & 0 & 0 \\ 0 & 0 & 0 & 0 & 0 & 0 \end{pmatrix} : d\underline{\underline{\varepsilon}}^p \tag{44}$$

By considering the assumption of plastic strain incompressibility, written as

$$d\varepsilon_{11}^p = -d\varepsilon_{22}^p - d\varepsilon_{33}^p \ , \tag{45}$$

it becomes possible to reorganize the components of the operator in a manner that resembles the shape of the ALO operator, *i.e.*

$$d\underline{\underline{\sigma}}\Big|_{\text{Plast Corr}} = -\begin{pmatrix} 0 & 0 & 0 & 0 & 0 & 0 \\ 0 & Y_{22}+Y_{11} & Y_{11} & 0 & 0 & 0 \\ 0 & Y_{11} & Y_{33}+Y_{11} & 0 & 0 & 0 \\ 0 & 0 & 0 & Y_{23} & 0 & 0 \\ 0 & 0 & 0 & 0 & 0 & 0 \\ 0 & 0 & 0 & 0 & 0 & 0 \end{pmatrix} : d\underline{\underline{\varepsilon}}^p \tag{46}$$

The equation involving the plastic correction with the Buczynski-Glinka heuristic takes the following final form

$$d\underline{\underline{\sigma}}\Big|_{\text{Plast Corr}} = -\underline{\underline{\underline{\underline{L}}}}^{BG} : d\underline{\underline{\varepsilon}}^p \ . \tag{47}$$

Nevertheless, the formulation of the components of this new operator can be simplified to facilitate the identification, by factorizing by 2 μ

$$\underline{\underline{\underline{\underline{L}}}}^{BG} = 2\ \mu \begin{pmatrix} 0 & 0 & 0 & 0 & 0 & 0 \\ 0 & (Y_{22}+Y_{11})\ \frac{1}{2\ \mu} & Y_{11}\ \frac{1}{2\ \mu} & 0 & 0 & 0 \\ 0 & Y_{11}\ \frac{1}{2\ \mu} & (Y_{33}+Y_{11})\ \frac{1}{2\ \mu} & 0 & 0 & 0 \\ 0 & 0 & 0 & Y_{23}\ \frac{1}{2\ \mu} & 0 & 0 \\ 0 & 0 & 0 & 0 & 0 & 0 \\ 0 & 0 & 0 & 0 & 0 & 0 \end{pmatrix} \tag{48}$$

The previous equation allows to rewrite Buczynski-Glinka heuristic under the same formalism as the ALO method (Eq. 17). In this expression, $\underline{\underline{\underline{\underline{L}}}}^{BG}$ is written as a function of the various Y_{ij} components, which can be expressed as

$$\begin{aligned} Y_{ij}\ \frac{1}{2\ \mu} &= \frac{\Delta s_{ij}\ \frac{1}{2\ \mu}}{\frac{\Delta s_{ij}}{2\ \mu} + \Delta e_{ij}} \\ &= \frac{\Delta e_{ij}^e}{\Delta e_{ij}^e + \Delta e_{ij}} \\ &= \frac{\Delta e_{ij}^e}{2\ \Delta e_{ij}^e + \Delta e_{ij}^p} \\ &= \frac{1}{2 + \frac{\Delta e_{ij}^p}{\Delta e_{ij}^e}} \quad . \end{aligned} \tag{49}$$

It should be noted that the form of $\underline{\underline{\underline{\underline{L}}}}^{BG}$ operator obtained after the different operations is similar to the form of the adjustable localization operator method, although the path to justify it is very different : Buczynski-Glinka method relies on an energetic approach whereas the ALO method is

based on a scale transition approach. Looking closer, the same zero components are obtained and $\underline{\underline{\underline{\underline{L}}}}^{BG}$ operator is necessarily symmetric whereas this is not mandatory with the ALO. Another main difference is that the components of $\underline{\underline{\underline{\underline{L}}}}^{BG}$ are non-constant, even for proportional loading.

This succession of equations makes it possible to rewrite the formalism of the plastic correction equation of the Buczynski-Glinka method. A mathematical operator is introduced to facilitate the writing of the equation in this particular case. The term-to-term product of two matrices of the same dimension is defined by the sign " $*$ ". Let $(\underline{\underline{A}}, \underline{\underline{B}})$ be two matrices of dimensions (i, j), the term-to-term product is defined by

$$\underline{\underline{C}} = \underline{\underline{A}} * \underline{\underline{B}} \ , \tag{50}$$

such that

$$C_{ij} = A_{ij} \ B_{ij} \ . \tag{51}$$

Moreover, the $\underline{\underline{F}}^{BG}$ tensor is defined, using Eq. 27, such that

$$F_{ij} = \frac{1}{\sqrt{1 + (\frac{\mu \Delta \varepsilon^p_{ij}}{\Delta S_{ij}})^2}} \ . \tag{52}$$

Hence, for the Buczynski-Glinka method, the evolution of the increment $d\underline{\underline{\sigma}}$ is written

$$d\underline{\underline{\sigma}} = \underline{\underline{F}}^{BG} * d\underline{\underline{\Sigma}} - \underline{\underline{\underline{\underline{L}}}}^{BG} : d\underline{\underline{\varepsilon^p}} \ . \tag{53}$$

This equation (Eq. 53) shows that the Buczynski-Glinka approach differs from the ALO approach in two ways:

- First, the coefficients of the localization operator $\underline{\underline{\underline{\underline{L}}}}^{BG}$ are variable;
- Second, the presence of the tensor $\underline{\underline{F}}^{BG}$ linked to the stress tensor under elastic assumption $\underline{\underline{\Sigma}}$.

Thereafter, a simple plane strain test simulation is run to highlight the influence of the tensor $\underline{\underline{F}}^{BG}$ on the predicted mechanical response. The simulation without this tensor is noted BG_{mod} and the equation then becomes

$$d\underline{\underline{\sigma}} = d\underline{\underline{\Sigma}} - \underline{\underline{\underline{\underline{L}}}}^{BG_{mod}} : d\underline{\underline{\varepsilon^p}} \ . \tag{54}$$

This method is not meant to be used as an alternative method for mechanical predictions but only to understand the role of this part of the equation.

3.4. Plane strain simulation on a double notched specimen

Two simulations are carried out in order to study the influence of the $\underline{\underline{F}}^{BG}$ tensor. These simulations are run on a double-notched specimen (figure 4), under the assumption of plane strain. In this simulation, the behavior is assumed to be perfect elastoplastic, with a yield stress of 300 MPa and a Young modulus E of 210 GPa.

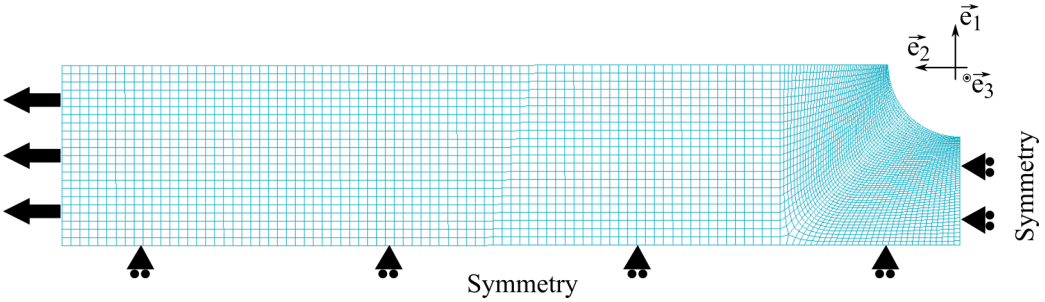

Figure 4: Quarter of a double-notched specimen for finite element modelling

Figure 5 compares the response of the different simulations to the FEA reference in different spaces. Figure 5a which is a classical stress/strain graph shows that the two responses of the analyzed method (BG and BG_{mod}) appear relatively close. The two curves overlap for both direction 2 and direction 3. However, while it is interesting to observe the stress/strain response, this graph is not suitable for comparing the methods. The next two graphs provide a clearer illustration of the differences between the two methods.

In figure 5b, the correction, which represents the difference between the von Mises stress predicted under elastic assumption and the stress obtained using an elastoplastic assumption, is plotted (similarly to figure 2). Both methods predict a non-linear evolution; however, the BG_{mod} method deviates from the BG method. This graph also reveals that a larger plastic deformation is obtained when the $\underline{\underline{F}}^{BG}$ tensor is removed from the equation.

In the last graph, figure 5c, it becomes apparent that neither of the two proposed methods captures the evolution of the loading path as predicted by the FEA reference, specifically the σ_{33}/σ_{22} stress ratio. Previous studies have demonstrated that the ALO method is capable of representing this evolution. This observation emphasizes that a non-linear version of the ALO method would combine the advantages of both the introduced methods: a nonlinear correction with an adaptive loading path.

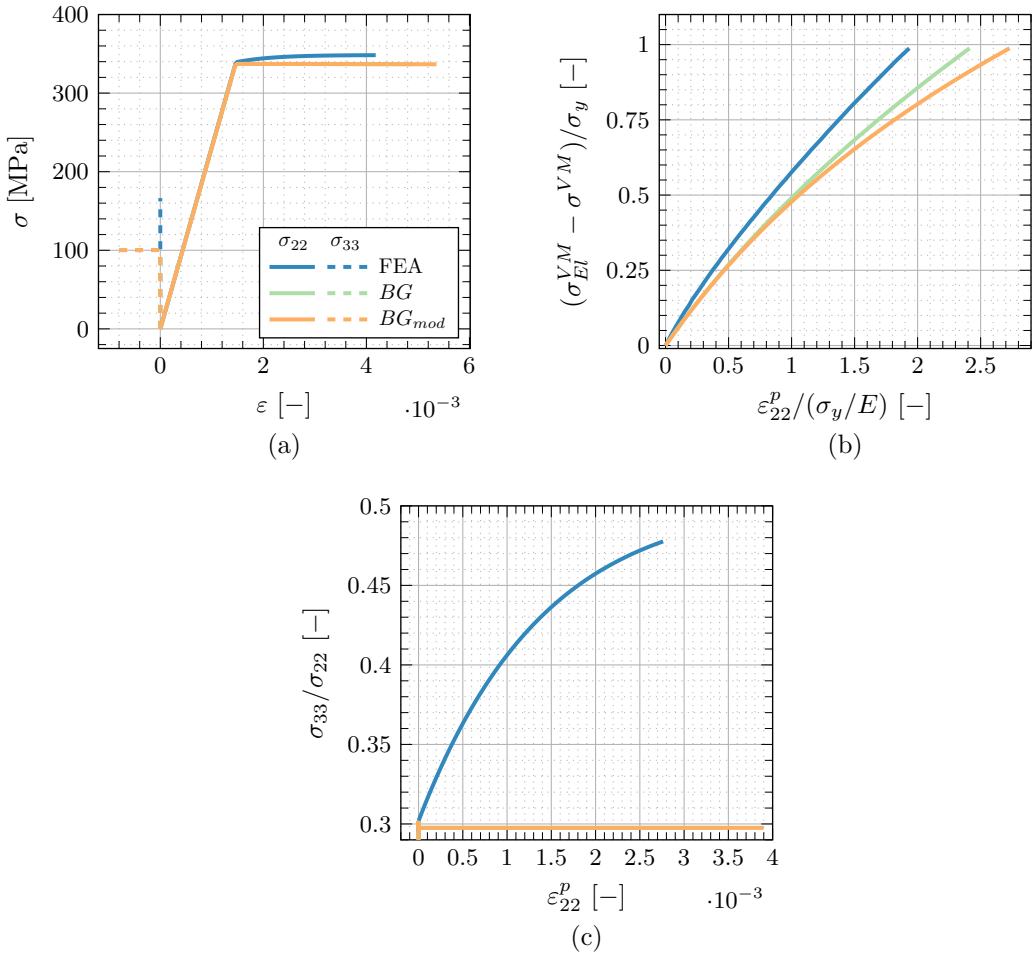

Figure 5: Comparison of the numerical predictions of Buczynski-Glinka (a) stress-strain curves, (b) deviation from the von Mises equivalent stress of the elastic simulation, (c) evolution of the stress ratio

The non-linear evolution of the BG method is enabled by the plasticity-induced variation of the z_{ij} coefficients, whereas in the classic ALO method, these parameters are fixed.

The graph provides a visualization of the parameter evolution during the numerical simulation. Several observations can be made. The first one is that z_{22} and z_{33} parameters are equal . Then, as soon as plasticity occurs, the values of z_{22} and z_{33} decrease. While a similar trend is observed for z_{22} and z_{33}, the graph also demonstrates a consistent factor of 2 in relation to the evolution of the parameter z_{23}.

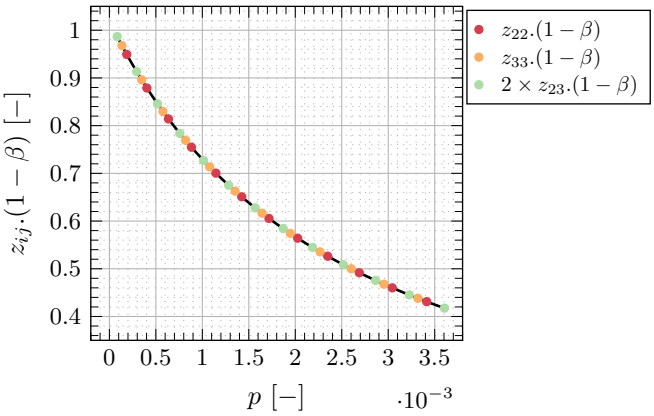

Figure 6: Evolution of Buczynski-Glinka parameters

One last important observation that can be seen in figure 5, is that the ratio σ_{33}/σ_{22} remains constant with the BG and BG_{mod} methods. This behavior is a direct consequence of the method's formulation. In equation Eq. 17, assuming the plastic flow strain tensor is normal to the von Mises surface, it can be replaced by

$$d\underline{\underline{\varepsilon}}^p = \frac{3}{2} d\lambda \frac{1}{\sigma^{VM}} \underline{\underline{\underline{\underline{J}}}} : \underline{\underline{\sigma}} \, . \tag{55}$$

Here, $d\lambda$ represents the cumulated plasticity, σ^{VM}_{loc} is the von Mises equivalent stress, and $\underline{\underline{\underline{\underline{J}}}}$ denotes the deviatoric projector. This substitution leads to the equation

$$d\underline{\underline{\sigma}} = d\underline{\underline{\Sigma}} - \frac{3}{2} d\lambda \frac{1}{\sigma^{VM}} \underline{\underline{\underline{\underline{L}}}}^{ALO} : \underline{\underline{\underline{\underline{J}}}} : \underline{\underline{\sigma}} \, . \tag{56}$$

The doubly contraction product between $\underline{\underline{\underline{\underline{L}}}}^{ALO}$ et $\underline{\underline{\underline{\underline{J}}}}$ can be expressed as

$$\underline{\underline{\underline{\underline{L}}}}^{ALO} : \underline{\underline{\underline{\underline{J}}}} = \frac{2}{3} 2\mu(1-\beta) \underline{\underline{\underline{\underline{L'}}}} \, , \tag{57}$$

where

$$\underline{\underline{\underline{\underline{L'}}}} = \begin{pmatrix} 0 & 0 & 0 & 0 & 0 & 0 \\ -\frac{z_{22}+z_{23}}{2} & z_{22} - \frac{z_{23}}{2} & z_{23} - \frac{z_{22}}{2} & 0 & 0 & 0 \\ -\frac{z_{33}+z_{32}}{2} & z_{23} - \frac{z_{33}}{2} & z_{33} - \frac{z_{32}}{2} & 0 & 0 & 0 \\ 0 & 0 & 0 & \frac{3}{2} z_{44} & 0 & 0 \\ 0 & 0 & 0 & 0 & 0 & 0 \\ 0 & 0 & 0 & 0 & 0 & 0 \end{pmatrix}_{(\vec{e_1},\vec{e_2},\vec{e_3})} \, . \tag{58}$$

Figure 6 shows that a factor 2 exists between the parameters z_{22}, z_{33} and the parameter z_{23} and which implies that $z_{23} - \frac{z_{22}}{2} = 0$ and $z_{32} - \frac{z_{33}}{2} = 0$. Therefore, the stress ratio is constant as illustrated in figure 5. The components that appeared in the first column of $\underline{\underline{\underline{\underline{L'}}}}$ are not of interest in the rest of this work, because the stress is equal to 0 on the free surface ($\sigma_{11} = 0$).

This section has illustrated the energetic method of Buczynski-Glinka and its non-linear plastic correction. Through the development of equations, it has been shown that it is possible to derive a localization operator with the same form as the adjustable localization operator. However, the Buczynski-Glinka method does not allow the stress ratio to evolve because of the relations between certain parameters ($z_{22} = z_{33} = 2.z_{23}$), which differs from previous methods in the literature [31, 33, 42].

Based on these findings, a plasticity-dependent adjustable localization operator method, combining Darlet's heuristic and the non-constant coefficients of the Buczynski-Glinka method, will be proposed thereafter. For the sake of simplicity, the plasticity-dependent ALO will be called non-linear ALO and denoted ALO^{NL}.

4. Proposal for a plasticity-dependent Adjustable Localization Operator

4.1. Formalism of the nonlinear adjustable localization operator

To maintain the formalism and the writing of the localization law for an adjustable localization operator, the corrective term $\underline{\underline{F}}^{BG}$ derived from Buczynski-Glinka heuristic is not retained. It has been shown that this factor has a small influence on the predictions and is therefore not necessary. Following a similar approach as in Eq. 17, the localization law for the nonlinear adjustable localization operator is proposed as

$$d\underline{\underline{\sigma}} = d\underline{\underline{\Sigma}} - \underline{\underline{\underline{\underline{L}}}}^{ALO^{NL}} : d\underline{\underline{\varepsilon}}^{p} \ . \tag{59}$$

The parameters z_{22} and z_{33} of this operator are defined using expressions similar to the operator $\underline{\underline{\underline{\underline{L}}}}^{BG}$ (Eq. 48)

$$z_{22}^{NL}.(1-\beta) = (Y_{22} + Y_{11})\ \frac{1}{2\ \mu} = \frac{1}{2 + \frac{\Delta e_{22}^{p}}{\Delta e_{22}^{e}}} + \frac{1}{2 + \frac{\Delta e_{11}^{p}}{\Delta e_{11}^{e}}} \quad , \tag{60}$$

$$z_{33}^{NL}.(1-\beta) = (Y_{33} + Y_{11})\ \frac{1}{2\ \mu} = \frac{1}{2 + \frac{\Delta e_{33}^{p}}{\Delta e_{33}^{e}}} + \frac{1}{2 + \frac{\Delta e_{11}^{p}}{\Delta e_{11}^{e}}} \quad , \tag{61}$$

and the parameter z_{44} is fixed such that

$$z_{44}^{NL}(1-\beta) = 0.5 \ \ . \tag{62}$$

As in the rest of the paper, the notation Δ designates the variation of variables with respect to a memory point (figure 3).

The parameter z_{23} is re-evaluated at each loading increment using Darlet's heuristic [33], with the equation given below

$$z_{23}^{NL} = \frac{z_{22}^{NL} AD - z_{33}^{NL} BC + z_{33}^{NL} \frac{AC}{2} - z_{22}^{NL} \frac{BD}{2}}{AC - BD + \frac{AD}{2} - \frac{BC}{2}} \ . \tag{63}$$

where the variables A, B, C and D are equal to

$$\begin{cases} A = \Sigma_{22}^{\nu \approx 0.5} \\ B = \Sigma_{33}^{\nu \approx 0.5} \\ C = \Sigma_{22}^{\nu} \\ D = \Sigma_{33}^{\nu} \end{cases} . \tag{64}$$

Σ_{22}^{ν} and Σ_{3}^{ν} are the stress tensor components at the critical point in directions 2 and 3 that are obtained by performing an elastic simulation that uses the material elastic properties (Young's modulus and Poisson's ratio ν). $\Sigma_{22}^{\nu \approx 0.5}$ and $\Sigma_{22}^{\nu \approx 0.5}$ are the same quantities obtained by performing an elastic simulation with modified material elastic properties. The Young's modulus is not modified but the Poisson's ratio is set to $\nu = 0.495$, to simulate the isochorous behavior of plastic deformations [32].

The non-linear plasticity-dependent operator ALO^{NL} is examined under various loading conditions to assess the impact of the non-linear plastic correction compared with the Buczynski-Glinka method and the previous linear ALO method [42] denoted as ALO^{L}. The identification of parameters follows Darlet's heuristic. The parameter z_{23} is identified using Equation 63, while the parameters z_{22} and z_{33} are constants and equal

$$z_{22}^{L}(1-\beta) = z_{33}^{L}(1-\beta) = 0.94 . \tag{65}$$

As the non-linear behavior is accounted for by the z_{22} and z_{33} terms, there is no need to modify the z_{44} parameter. Therefore, the parameter z_{44}^{L} is set equal to z_{44}^{NL}.

5. Method assessment on multiaxial loadings

5.1. Structure, material properties and loadings

The non-linear ALO method ALO^{NL} is applied to a specific structure depicted in figure 7. This structure exhibits a 3 mm displacement between its rotational axis and the rotational axis of the groove. As a result, a single stress concentration point is formed on the surface of the structure, regardless of the combination of tensile and torsional loads applied.

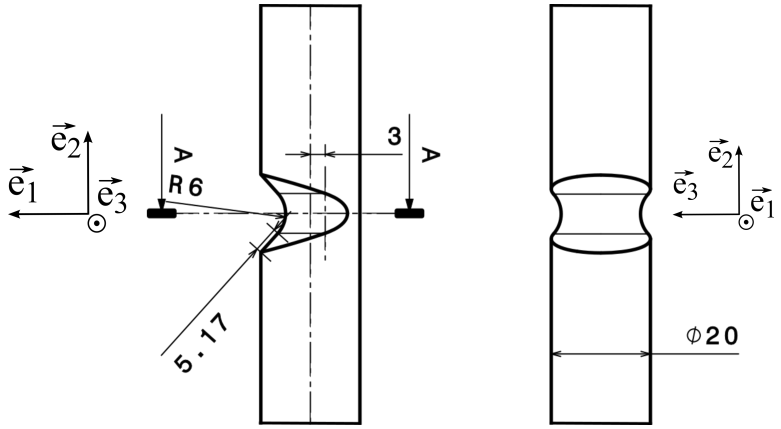

Figure 7: Notched structure for multiaxial loadings

The simulated fictitious material exhibits an elastoplastic behavior with two combined kinematic hardenings. The multi-hardening model proposed by Chaboche [39] is used, with the two kinematic hardenings following the Armstrong-Frederick model [48]. The expressions for these kinematic hardenings, denoted as $\underline{\underline{X_i}}$, are as follows:

$$d\underline{\underline{X_i}} = \frac{2}{3} C_i d\underline{\underline{\varepsilon_p}} - \gamma_i \underline{\underline{X_i}} dp \ . \tag{66}$$

The yield surface f is governed by the following equation

$$f(\underline{\sigma}, \underline{\underline{X}}) = J_2(\underline{\sigma} - \underline{\underline{X}}) - \sigma_y \leq 0 \ . \tag{67}$$

The material properties used in the simulation are provided in table 3.

Behavior	Parameters	Value
Elastic	σ_y [MPa]	300
	E [MPa]	210 000
	ν [-]	0.3
Nonlinear kinematic hardening X_1	C_1 [MPa]	50 000
	γ_1 [-]	200
Linear kinematic hardening X_2	C_2 [MPa]	800
	γ_2 [-]	0

Table 3: Parameters of the constitutive equations

Two distinct simulations are performed to investigate different aspects of the proposed methods. First, a monotonic and uniaxial tensile test is simulated to highlight the advantages of Darlet's heuristic for local multiaxial loading conditions, in comparison to the Buczynski-Glinka method.

Subsequently, a cyclic simulation is conducted to demonstrate the benefits of the non-linear ALO method compared to the previous identification strategy proposed by Darlet [42]. This cyclic loading scenario allows for a comprehensive evaluation of the non-linear method's performance and its ability to enhance the material behavior predictions during cyclic loading, in comparison with the linear approach.

5.2. Results

5.2.1. Comparison between BG and ALO^{NL} methods

The first loading scenario investigated in this study is a monotonic uniaxial tension. Figure 8 presents the numerical predictions obtained using both the Buczynski-Glinka (BG) method and the ALO^{NL} method.

Figure 8a shows that the results obtained by the various methods are very close to each other in the stress/strain space although σ_{33} is slightly underestimated by the Buczynski-Glinka method. This suggests that the ALO^{NL} method provides more accurate predictions in capturing the behavior of the material under uniaxial tension.

The evolution of the stress ratio is illustrated in figure 8b, highlighting the importance of the Darlet heuristic. The stress ratio does not remain constant and matches the evolution of the finite element method, indicating the capability of the ALO^{NL} method to capture the stress ratio behavior.

Figure 8c allows us to highlight the deviation from the equivalent von Mises stress between the elastic simulation and the elastoplastic response obtained with the different method. It shows that all methods provide a non-linear correction, confirming the improvement of the ALO^{NL} method as compared to the ALO^{L} method. ALO^{NL} results evolution is closer to the finite element method than the energetic method. This is emphasized by figure figure 8d which shows the percentage of error with respect to the finite element method, made by Buczynksi-Glinka and ALO^{NL} methods in the correction. This percentage denoted as δ^{EF} remains small for both methods.

Overall, the analysis of figure 8 demonstrates the effectiveness of the ALO^{NL} method, particularly in capturing the stress ratio behavior and providing accurate predictions compared to the Buczynski-Glinka method and the finite element method.

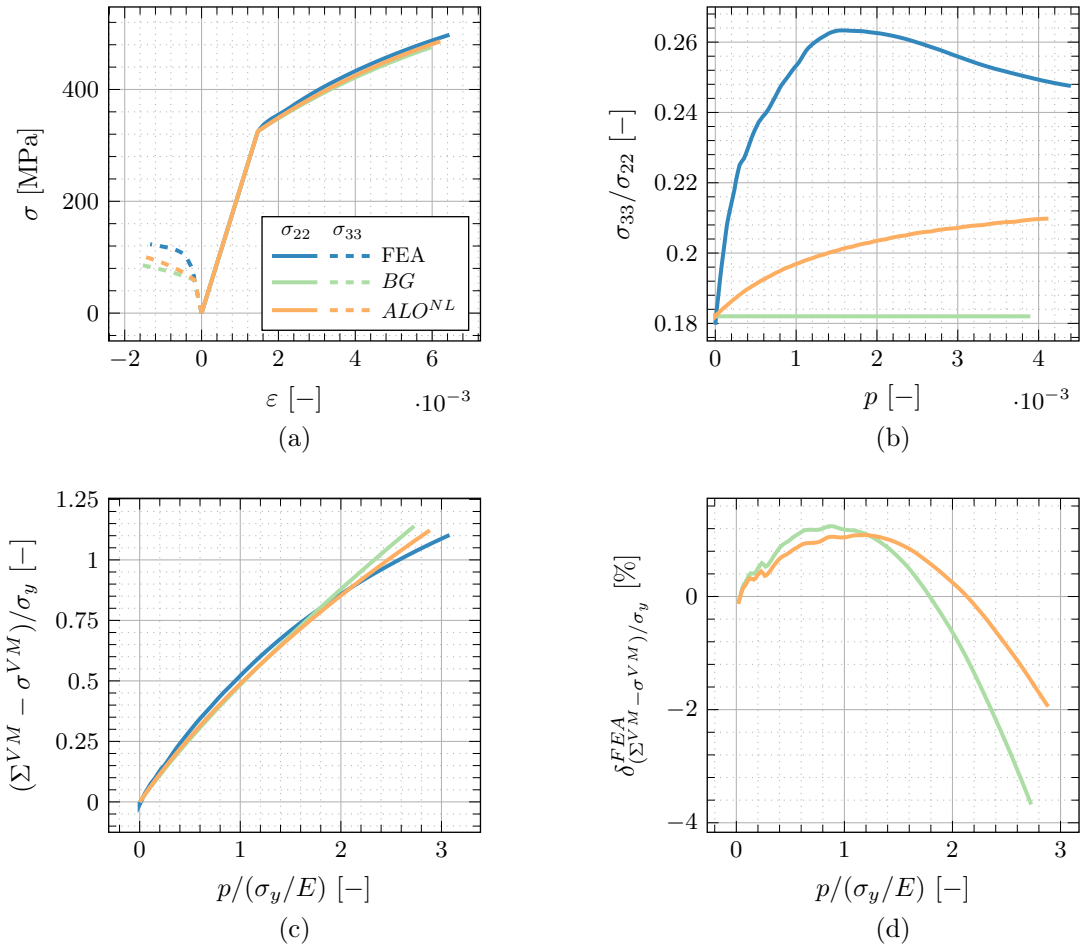

Figure 8: Comparison of the numerical predictions : (a) stress-strain curves, (b) evolution of the stress ratio, (b) deviation from the von Mises equivalent stress of the elastic simulation, (d) error with finite element method deviation from the equivalent stress of the elastic simulation

5.2.2. Cyclic simulation and comparison with the ALO^L method

The second loading is a cyclic loading with a load ratio of $R = -0.3$. The numerical predictions obtained using the ALO^{NL} method and with the previous identification method ALO^L [42] are compared to the FEA method. Figure 9 illustrates the results.

Figures 9a et 9b show that the FEA predicts a slight accommodation during the cyclic loading. This phenomenon is correctly predicted with the ALO^{NL} method as no additional ratcheting phenomenon is observed. This suggests that the ALO^{NL} method effectively captures the cyclic behavior without excessive plastic deformation accumulation. In addition, it can be seen that despite a nominal load ratio of $R = -0.3$, the local load ratio decreases progressively to $R = -1$. These two graphs show that the ALO approach can capture this effect properly, specifically in the main direction of solicitation.

The numerical results obtained with the ALO^{NL} method demonstrate an improvement compared to the linear correction of the previous identification method ALO^L, as shown in figure 9c. Again, this result is emphasized in figure 9d that represent the error percentage of the ALO method correction compared to FEA correction , denoted as δ^{EF}. The ALO^{NL} method correction exhibits a smaller error (less than 2%) than the linear version (error close to 10%).

In summary, the analysis of figure 9 demonstrates that the ALO^{NL} method performs well in the context of cyclic loading. It shows improved results compared to the previous identification method ALO^L, as evidenced by the reduced deviation from the elastic simulation and the small error with respect to the finite element method.

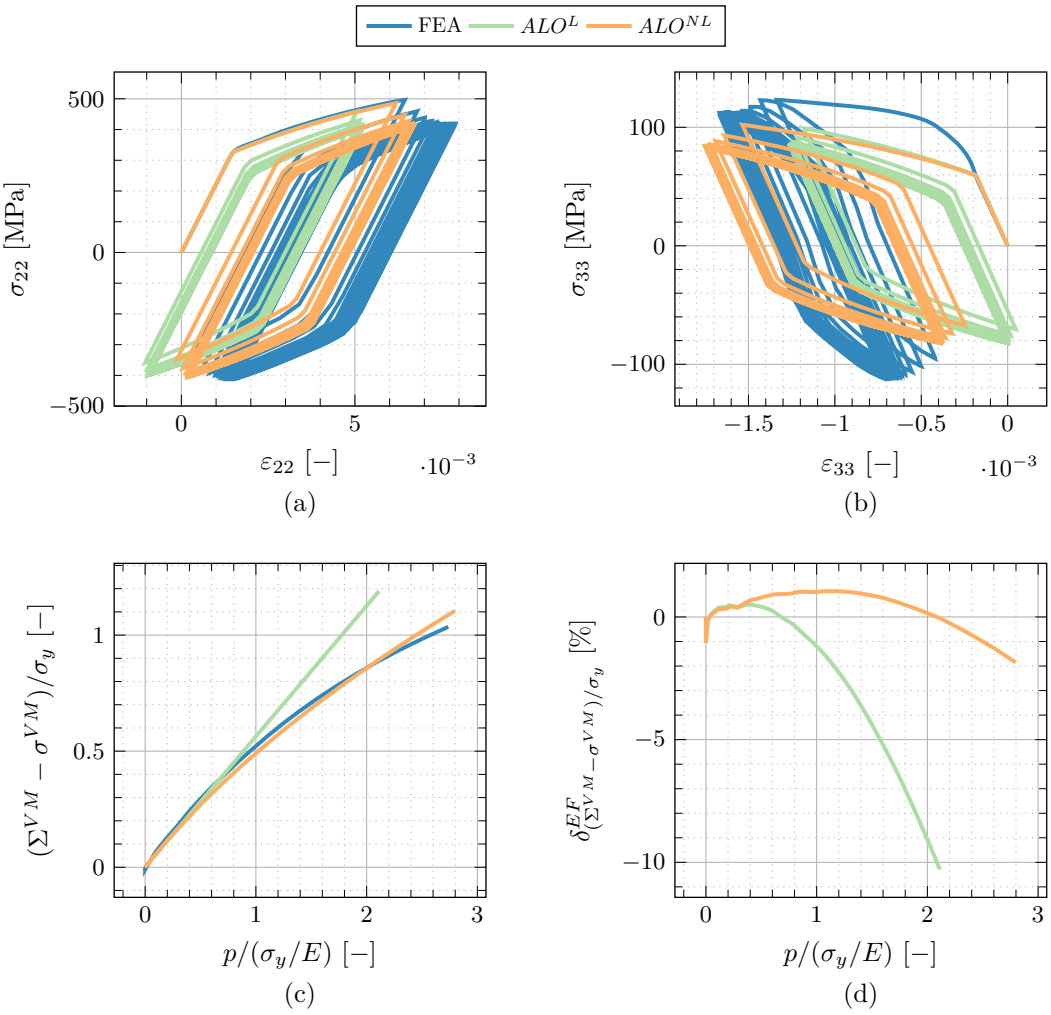

Figure 9: Comparison of the numerical predictions with the linear method (a) stress-strain curves, (b) evolution of the stress ratio, (b) deviation from the von Mises equivalent stress of the elastic simulation, (d) error with finite element method deviation from the equivalent stress of the elastic simulation

6. Conclusion

The main objective of this paper was to propose a formulation of the Adjustable Localization Operator operator inspired by energetic methods to extend the capability of the method to non-linear correction prediction. The heuristic developed by Buczynski-Glinka to extend Neuber's rule to multiaxial loadings was used, leading to the formulation of an ALO method with non-constant parameters and a non-linear plastic correction. It was pointed out that although the energetic methods directly provide a non-linear correction, they cannot represent the FEA predicted evolution of the σ_{22}/σ_{33} stress ratio.

The advantages of the ALO^{NL} method compared to the previous linear version were demonstrated through the analysis of cyclic tensile loading. The results showed that the proposed method provides more accurate predictions of the local stress and strain state compared with the previous linear version. Furthermore, the method's efficiency, requiring only two elastic simulations, makes it practical for real-world engineering applications.

Further investigations could be conducted to analyze the behavior of the non-linear ALO method under more complex loadings, particularly non-proportional tension-torsion loading. While previous studies have demonstrated the effectiveness of the ALO method with the linear operator in such scenarios, the specific contribution and performance of the non-linear operator in these cases remain to be validated. Additionally, it would be valuable to test the non-linear ALO method capability to predict more complex behavior, such as ratcheting or softening, using adequate behavior laws.

As a final conclusion, it is worth to recall that the ALO method has been developed and refined by various research teams over the past two decades, addressing different engineering challenges such as stress ratio prediction, mean stress evolution, visco-plastic behavior, and anisotropic behavior, among others. The aim of all these research projects was to provide accurate predictions for structural analysis while significantly reducing computational time compared to the reference finite element analysis (FEA) method. The success of the ALO method lies in its formalism, which is based on an analogy between the confined plasticity zone and Eshelby's work. This analogy provides a robust and flexible framework that has allowed to address this wide variety of problems, using variations of the method.

References

[1] H. Neuber, Theory of Stress Concentration for Shear - Strained Prismatical Bodies With Arbitrary Nonlinear Stress - Strain Law, J. of Applied Mechanics 28 (1) (1961) 544–551.

[2] Walker, Multiaxial Stress-Strain Approximations for Notch Fatigue Behavior, Journal of Testing and Evaluation 5 (1977) 106–113.

[3] S. Savalle, J. P. Culié, Méthodes de Calcul Associées aux Lois de Comportement Cyclique et d'Endommagement, La Recherche Aérospatiale 5 (1978) 263–278.

[4] K. Molski, G. Glinka, A Method of Elastic-Plastic Stress and Strain Calculation at a Notch Root, Materials Science and Engineering 50 (1) (1981) 93–100. doi:10.1016/0025-5416(81)90089-6.

[5] G. Glinka, Energy Density Approach to Calculation of Inelastic Strain-Stress near Notches and Cracks, Engineering Fracture Mechanics 22 (3) (1985) 485–508. doi:https://doi.org/10.1016/0013-7944(85)90148-1.

[6] G. Glinka, Calculation of Inelastic Notch-tip Strain-Stress Histories under Cyclic Loading, Engineering Fracture Mechanics 22 (5) (1985) 839–854. doi:https://doi.org/10.1016/0013-7944(85)90112-2.

[7] H. B. Dhia, Multiscale mechanical problems: the Arlequin method, Comptes Rendus De L Academie Des Sciences Serie Ii Fascicule B-mecanique Physique Astronomie 12 (1998) 899–904.

[8] F. Feyel, J.-L. Chaboche, FE2 Multiscale Approach for Modelling the Elastoviscoplastic Behaviour of Long Fibre SiC/Ti Composite Materials, Computer Methods in Applied Mechanics and Engineering 183 (3) (2000) 309–330. doi:10.1016/S0045-7825(99)00224-8.
URL https://www.sciencedirect.com/science/article/pii/S0045782599002248

[9] A. Llau, L. Jason, F. Dufour, J. Baroth, Adaptive Zooming Method for the Analysis of Large Structures with Localized Nonlinearities, Finite Elements in Analysis and Design 106 (2015) 73–84. doi:10.1016/j.finel.2015.07.011.
URL https://www.sciencedirect.com/science/article/pii/S0168874X15001146

[10] W. V. Paepegem, J. Degrieck, P. D. Baets, Finite element approach for modelling fatigue damage in fibre-reinforced composite materials, Composites Part B-engineering 32 (2001) 575–588.

[11] R. Desmorat, Fast Estimation of Localized Plasticity and Damage by Energetic Methods, International Journal of Solids and Structures 39 (12) (2002) 3289–3310. doi:https://doi.org/10.1016/S0020-7683(02)00002-1.

[12] H. F. Maitournam, B. Pommier, J. J. Thomas, Détermination de la Réponse Asymptotique d'une Structure Anélastique sous Chargement Thermomécanique Cyclique, C.R. Mécanique 330 (2002) 703–708.

[13] B. Pommier, Détermination de la réponse asymptotique d'unestructure anélastique soumise à un chargementthermomécanique cyclique, Ph.D. thesis, Ecole Polytechnique (2003).

[14] F. Comte, H. Maitournam, P. Burry, T. Mac Lan Nguyen, A Direct Method for the Solution of Evolution Problems, Comptes Rendus Mécanique 334 (5) (2006) 317–322. doi:https://doi.org/10.1016/j.crme.2006.02.007.

[15] D. Ye, O. Hertel, M. Vormwald, A Unified Expression of Elastic-Plastic Notch Stress-Strain Calculation in Bodies Subjected to Multiaxial Cyclic Loading, International Journal of Solids and Structures 45 (24) (2008) 6177–6189, cited By 79. doi:10.1016/j.ijsolstr.2008.07.012.

[16] S. Kaulmann, M. Ohlberger, B. Haasdonk, A New Local Reduced Basis Discontinuous Galerkin Approach for Heterogeneous Multiscale Problems, Comptes Rendus Mathematique 349 (2011) 1233–1238.

[17] D. B. P. Huynh, D. J. Knezevic, A. T. Patera, A Static Condensation Reduced Basis Element Method: Approximation and a Posteriori Error Estimation, Mathematical Modelling and Numerical Analysis 47 (2013) 213–251.

[18] D. Ryckelynck, K. Lampoh, S. Quilicy, Hyper-Reduced Predictions for Lifetime Assessment of Elasto-Plastic Structures, Meccanica 51 (2) (2016) 309–317. doi:10.1007/s11012-015-0244-7.
URL https://doi.org/10.1007/s11012-015-0244-7

[19] A. Ince, G. Glinka, A Numerical Method for Elasto-Plastic Notch-Root Stress–Strain Analysis, The Journal of Strain Analysis for Engineering Design 48 (4) (2013) 229–244. doi:10.1177/0309324713477638.

[20] M. A. Meggiolaro, J. T. P. D. Castro, L. F. Martha, L. F. N. Marques, On the Estimation of Multiaxial Elastoplastic Notch Stresses and Strains under In-Phase Proportional Loadings, International Journal of Fatigue 100 (2017) 549–562, cited By 9. doi:10.1016/j.ijfatigue.2016.12.038.

[21] M. Bhattacharyya, A model reduction approach in space and time for fatigue damage simulation, Ph.D. thesis, LMT (2018).

[22] O. Sally, F. Laurin, C. Julien, R. Desmorat, F. Bouillon, An efficient computational strategy of cycle-jumps dedicated to fatigue of composite structures, International Journal of Fatigue 135 (2020) 105500. doi:10.1016/j.ijfatigue.2020.105500.
URL https://www.sciencedirect.com/science/article/pii/S0142112320300311

[23] A. T. Htoo, Y. Miyashita, Y. Otsuka, Y. Mutoh, S. Sakurai, Variation of Local Stress Ratio and Its Effect on Notch Fatigue Behavior of 2024-T4 Aluminum Alloy, International Journal of Fatigue 88 (2016) 19–28, cited By 15. doi:10.1016/j.ijfatigue.2016.03.001.

[24] A. T. Htoo, Y. Miyashita, Y. Otsuka, Y. Mutoh, S. Sakurai, Notch Fatigue Behavior of Ti-6Al-4V Alloy in Transition Region between Low and High Cycle Fatigue, International Journal of Fatigue 95 (2017) 194–203, cited By 18. doi:10.1016/j.ijfatigue.2016.10.024.

[25] H. Remes, J. Romanoff, I. Lillemäe, D. Frank, S. Liinalampi, P. Lehto, P. Varsta, Factors Affecting the Fatigue Strength of Thin-Plates in Large Structures, International Journal of Fatigue 101 (2017) 397–407, cited By 17. doi:10.1016/j.ijfatigue.2016.11.019.

[26] Y. Dong, Y. Garbatov, C. Guedes Soares, A Two-Phase Approach to Estimate Fatigue Crack Initiation and Propagation Lives of Notched Structural Components, International Journal of Fatigue 116 (2018) 523–534, cited By 16. doi:10.1016/j.ijfatigue.2018.06.049.

[27] B. Skallerud, S. K. Ås, N. S. Ottosen, A Gradient-Based Multiaxial Criterion for Fatigue Crack Initiation Prediction in Components with Surface Roughness, International Journal of Fatigue 117 (2018) 384–395, cited By 12. doi:10.1016/j.ijfatigue.2018.08.020.

[28] M. Schuscha, M. Leitner, M. Stoschka, G. Meneghetti, Local Strain Energy Density Approach to Assess the Fatigue Strength of Sharp and Blunt V-Notches in Cast Steel, International Journal of Fatigue 132, cited By 3 (2020). doi:10.1016/j.ijfatigue.2019.105334.

[29] P. Corigliano, V. Crupi, X. Pei, P. Dong, DIC-based Structural Strain Approach for Low-Cycle fatigue Assessment of AA 5083 Welded Joints, Theoretical and Applied Fracture Mechanics 116 (2021) 103090. doi:https://doi.org/10.1016/j.tafmec.2021.103090.

[30] C. Ronchei, A. Carpinteri, D. Scorza, A. Zanichelli, S. Vantadori, The RED Criterion for Fatigue Life Assessment of Metals under Non-Proportional Loading, International Journal of Fatigue 163 (2022) 107080. doi:https://doi.org/10.1016/j.ijfatigue.2022.107080.

[31] T. Herbland, G. Cailletaud, S. Quilici, H. Jaffal, A New Technique for the Fatigue Life Prediction in Notched Components, in: Cetim Senlis, 2009.

[32] A. Darlet, R. Desmorat, Stress Triaxiality and Lode Angle along Surfaces of Elastoplastic Structures, International Journal of Solids and Structures 67-68 (2015) 71–83.

[33] E. Gautier, B. Levieil, S. Calloch, A. Ezanno, C. Doudard, Improvement of the Adjustable Localization Operator Identification based on the Confined Plasticity Zone Shape for Multiaxial Elasto-Plastic Cyclic Predictions, International Journal of Solids and Structures 262-263 (2023) 112077. doi:10.1016/j.ijsolstr.2022.112077.
URL https://www.sciencedirect.com/science/article/pii/S0020768322005303

[34] M. Hoffmann, T. Seeger, A Generalized Method for Estimating Multiaxial Elastic-Plastic Notch Stresses and Strains Part 1: Theory, Journal of Engineering Materials and Technology, Transactions of the ASME 107 (4) (1985) 250–254.

[35] M. E. Barkey, D. F. Socie, K. J. Hsia, A Yield Surface Approach to the Estimation of Notch Strains for Proportional and Nonproportional Cyclic Loading, Journal of Engineering Materials and Technology 116 (2) (1994) 173–180.

[36] A. Moftakhar, A. Buczynski, G. Glinka, Elastic-Plastic Stress–Strain Calculation in Notched Bodies Subjected to Nonproportional Loading, International journal of fracture 70 (1995) 357–373.

[37] Gallerneau, Extension of Neuber's Rule to Stress Concentration in Multiaxial Viscoplasticity. In: 8th International Symposium on Plasticity and its Current Applications, in: Whistler (Canada), July 17–21, 2000.

[38] A. Buczynski, G. Glinka, An Analysis of Elasto-Plastic Strains and Stresses in Notched Bodies Subjected to Cyclic Non-Proportional Loading Paths 31 (2003) 265–283. doi:https://doi.org/10.1016/S1566-1369(03)80015-8.

[39] J.-L. Chaboche, A New Heuristic Method to Compute Local Stresses and Strains at Notch Tip for Multiaxial Stress States, Tech. rep., ONERA (2007).

[40] J. D. Eshelby, The Determination of the Elastic Field of an Ellipsoidal Inclusion, and Related Problems, The Royal Society (1957) 376–396.

[41] E. Kröner, Zur Plastischen Verformung des Vielkristalls, Acta Metallurgica 9 (2) (1961) 155–161.

[42] A. Darlet, Estimation Rapide en Surface de la Triaxialité des Contraintes et de la Plasticité : Application aux Disques et aux Aubes de Turbine des Turboréacteurs, Ph.D. thesis (2014).

[43] B. Levieil, F. Bridier, C. Doudard, D. Thevenet, S. Calloch, A. Ezanno, Numerical Simulation of Low-cycle Fatigue Behavior of Welded Joints for Naval Applications: Influence of Residual Stresses, Welding in the World 61 (3) (2017) 551–561. doi:10.1007/s40194-017-0453-x.

[44] B. Levieil, C. Doudard, D. Thevenet, F. Bridier, A. Ezanno, S. Calloch, An Original Simplified Method Based on the Use of an Adjustable Localization Operator for Low-Cycle Fatigue Life Predictions in the Case of Confined Plasticity, Theoretical and Applied Fracture Mechanics 104 (June) (2019) 102383.

[45] B. Levieil, C. Doudard, D. Thevenet, F. Bridier, A. Ezanno, S. Calloch, Taking Residual Stresses into Account in Low-Cycle Fatigue Design using the Adjustable Localisation Operator Method, International Journal of Fatigue 150, cited By 1 (2021). doi:10.1016/j.ijfatigue.2021.106322.

[46] J.-B. Le Bail, B. Levieil, S. Moyne, C. Doudard, S. Calloch, Extension of the Adjustable Localization Operator Method to Anisotropic Elasto-Plastic Behavior for Low-Cycle Fatigue Life Prediction, Journal of Engineering Materials and Technology 144 (4), 041002 (04 2022). doi:10.1115/1.4054289.

[47] M. Chouman, A. Gaubert, J.-L. Chaboche, P. Kanouté, G. Cailletaud, S. Quilici, Elastic-Viscoplastic Notch Correction Methods, International Journal of Solids and Structures 51 (18) (2014) 3025–3041, cited By 5. doi:10.1016/j.ijsolstr.2014.04.017.

[48] P.-J. Armstrong, C.-O. Frederick, A Mathematical Representation of the Multiaxial Baushinger Effect (1966).